Report Semesterproject: Noise characterisation of current-stabilised power supplies

Report Semesterproject: Noise characterisation of current-stabilised power supplies

Felix Borchers

September 9, 2024

Contents

1 Introduction

In this report we will detail some of the work done during the semesterproject with the Lattice Team of in Prof. Esslinger's group from March to June 2024. The main task was to measure the noise of different current sources. Beyond this some other smaller projects working on magnetic field measurements, temperature measurements of the coils and a test current ramp are reported as well.

2 Current Noise Measurement

As the main part of this report we will describe the results and methodology for measuring the current noise associated with the three power supplies (High-Finesse UCS70, Delta SM-6000, EA 9080-100) operated as current sources in the frequency region [10 Hz, 10 kHz]. These three power supplies will be used for Feshbach coils, evaporation coils and multiple purposes respectively. In an earlier paper [3] another group managed using feedback and feedforward to obtain a noise figure of 0.67ppm at $I_0 = 60\,\mathrm{A}$. No such noise reduction technique was implemented in our

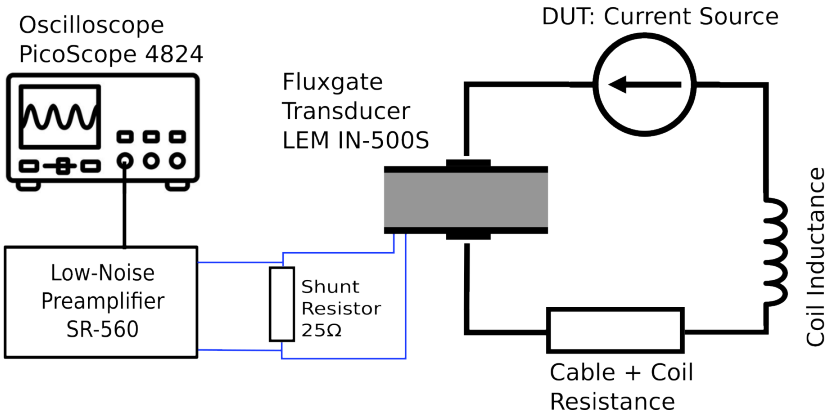

Figure 1: Current Measurement Set-up. Right: Primary circuit of current source and coil (represented by the inductance and resistance). Left: Secondary read-out circuit of the fluxgate transducer.

setup. The noise measurement consists of two main steps. First, measuring the current output by means of a transducer and second, calculating the corresponding power spectrum.

2.1 Measurement Set-up

Different to previous measurement using a simple shunt resistor set-up, we decided to measure the current using a closed-loop fluxgate transducer (LEM IN-500 S). This method allowed to monitor the current during the operation of a magnetic field coil by the current source without introducing an additional shunt resistor in the circuit. Different to the shunt resistor the fluxgate transducer picks up the magnetic flux of the current passing through a wire and produces a secondary (output) current proportional to the primary (input) current. For a brief summary of the working principle cf. [1]. A sketch of the full set-up is shown in Figure 1.

The primary circuit consisted of the current source under test connected to a magnetic-field coil $L = 15.6\,\mu\text{H}$ providing a resistance of $\sim 10\,\text{m}\Omega$. The magnetic-field coil was manufactured from a single piece of copper with 22 effective windings and 1cm effective radius. The low-resistance and integrated water cooling allowed to drive the coil at high currents above 300 A. The output current of the transducer was picked up as a voltage over a $25\,\Omega$ shunt resistor. Both the shunt resistor and the output current D-Sub to coax connector were faradaically shielded by metal boxes.

The voltage was amplified and band-pass filtered ($0.03\,\text{Hz} - 30\,\text{kHz}$) by a preamplifier (Stanford Research Instrument SR-560), which was operated in the "low-noise" mode with AC coupling. Finally, the signal was digitized by an oscilloscope (PicoScope 4824).

The conversion between the output voltage and the primary current is given by

$$I = \frac{N_s}{ARN_p} U \tag{1}$$

with N_s the number of secondary windings (750 for the LEM IN-500 S), A the gain of the preamplifier, R the resistance of the shunt resistor ($25\,\Omega$) and N_p the number of primary windings of the cable through the transducer.

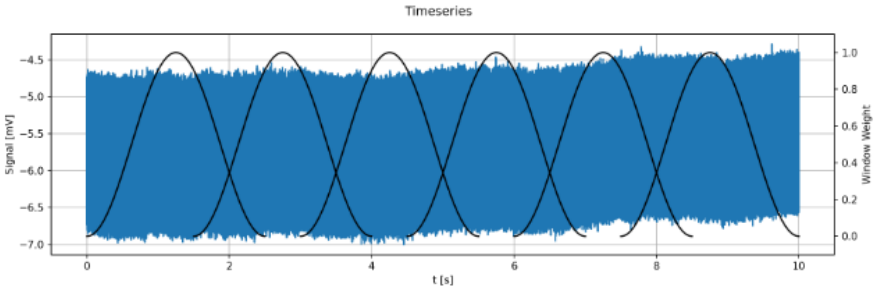

Figure 2: Time-series (blue) with window function segments indicated (black). Each "Gaussian" envelope describes a single windowing function. The windowing functions separate the time-series into overlapping intervals. The spectra obtained from the different intervals are averaged at the end.

2.2 Spectral Noise Density

The voltage data was collected as time-series by the oscilloscope. In the following we will discuss some of the necessary steps to obtain a noise spectral density from such data. A more complete overview may be found in [2].

The frequency spectrum of a time-series (x_k) is calculated by means of a discrete Fourier transform (DFT).

$$X_l = \sum_{k=0}^{n-1} x_k \mathrm{e}^{-2i\pi kl/n}, \quad x_k = \frac{1}{n} \sum_{l=0}^{n-1} X_l \mathrm{e}^{2i\pi kl/n} \tag{2}$$

with the normalization chosen such that the signal power is independent of the number of samples, as discussed in the referenced literature. Simply applying the DFT to the whole time-series, however, has some issues. First, the DFT assumes the time-series to be periodic. The mismatch of the time-series at the boundaries introduces leakage of frequencies incommensurate with the length of the time-series into multiple frequency bins. Second, the noise is random, wherefore the part of the spectrum capturing the noise will appear very noisy and be difficult to interpret.

To address the first issue, a windowing function can be applied. A windowing function depicted as one single "Gaussian" black contour in Figure 2, is zero at the boundaries, which recovers the periodicity and removes aliasing. A single windowing function does not necessarily cover the whole time-series. There exist different choices of window functions, with different trade-offs: flatness (accuracy of signal amplitudes), spectral leakage and roll-off (the degree to which neighbouring frequency bins contribute). In our case we decided to use the standard "Hanning" window.

The second issue with noise included in the spectrum can be addressed by simply averaging the Fourier transform. Given a single time-series, the data is divided into multiple sections defined by applying a window function, which might overlap with neigbouring sectors, as shown in Figure 2.The choice of overlap is a trade-off between utilizing the whole time-series and correlations between different sections. The optimal choice for the Hanning window is an overlap of 50%.

Given the Fourier transform of the time-series the power spectral density is obtained as

$$S_{xx}(f = l \cdot f_{\text{res}}) = \frac{2 \cdot |X_l|^2}{f_S \cdot S_2} \tag{3}$$

where S_2 is a normalization factor due to the applied window function. Note that the power is given in $\text{V}_{\text{rms}}^2/\text{Hz}$. We will refer to the root of the power spectral density ($\sqrt{S_{xx}(f)}$) as the linear spectral density, with corresponding units of $\text{V}_{\text{rms}}/\sqrt{\text{Hz}}$. The final power spectral density is the average over multiple power spectral densities. Note, that only power spectral densities and not linear spectral densities can be averaged. The above steps to obtain the power spectral density are comprehensively implemented in Python by the `scipy.signal.welch` function[1].

Given the power spectral density the noise equivalent current I_{noise} for some frequency interval $[f_1, f_2]$ is then

$$I_{\text{noise}} = \sqrt{\int_{f_1}^{f_2} S_{xx}(f) df} \tag{4}$$

The noise will often be quoted in terms of "ppm" which corresponds to the ratio of equivalent noise current in some frequency interval divided by the average set current I_{noise}/I_0.

2.3 Results

In this section we will discuss the results of the current measurements for the different current sources. First, we will discuss the effective bandwidth of the measuring set-up and discuss the noise inherent to the measurement. Second, we will discuss and compare the noise profiles of the different current sources. All later measurements were taken at a sampling frequency of $f_S = 400\,\text{kHz}$ and a 12+2bit resolution, which is equivalent to an effective sampling rate of $f_{S,\text{eff}} = 25\,\text{kHz}$. This relationship is explained in section 2.3.2 concerning digitization noise. The largest resolvable frequency is given by the Nyquist frequency $f_{\text{Ny}} = f_{S,\text{eff}}/2 = 12.5\,\text{kHz}$. A single time-series of 10 s was split into seven 2.5 s windowed intervals with 50% overlap. The frequency resolution was therefore $f_{\text{res}} = 0.4\,\text{Hz}$. For each setting the 14 spectra of two time-series were averaged. Note, the Nyquist frequency and frequency resolution cover the whole frequency interval of interest $[10\,\text{Hz}, 10\,\text{kHz}]$. In our measurements the choice of a large shunt resistor, while producing relatively larger voltages, limited us to a primary current of about 330 A, due to power limitations of the transducer output.

2.3.1 AC coupling high-pass and RL circuit low-pass filter

In this section we want to discuss two issues related to high- and low-pass filtering for the noise measurement. First, the AC-coupling constant of the preamplifier, which turns out to not influence the measurement as a high-pass filter for low frequencies. Second, the influence of the inductance of the coil in the primary circuit on the noise spectrum.

For the AC-coupling it is mentioned in the data-sheet that the behaviour is equivalent to a high-pass filter with cut-off frequency at 0.03 Hz, far below the 10 Hz of interest. We confirmed this behaviour by fitting an exponential decay to the amplifiers output voltage after applying a voltage jump by means of changing the current passing through the transducer. The data and fit are shown in Figure 3. The exponential decay yields a frequency of about $f_0 = 0.10\,\text{Hz}$ in agreement with the data sheet.

[1] https://docs.scipy.org/doc/scipy/reference/generated/scipy.signal.welch.html

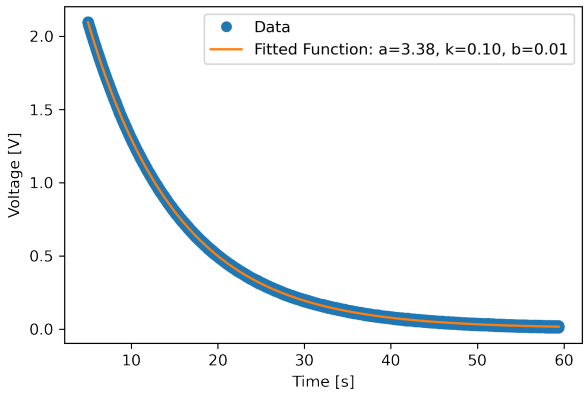

Figure 3: AC coupling frequency constant fit. Fit function: $f(t) = a\exp(-kt) + b$.

While the AC coupling does not affect the measurement the coil inductance does have a significant influence. For a simple series RL circuit the transfer function between the input voltage V_{in} and current I can be written

$$\left|\frac{I}{V_{\text{in}}}\right| = \frac{1}{\sqrt{R+\omega L}} \tag{5}$$

and displays a low-pass behaviour with cut-off frequency $\omega_c = R/L$. The resistance of the circuit for the Delta power supply including the inductance was estimated to be $R = 7\,\text{m}\Omega$. The inductance can be estimated by the formula [5]

$$L = \frac{0.32r^2N^2}{6r+9w+10t}\mu\text{H}, \quad [r] = [w] = [t] = \text{cm} \tag{6}$$

with r the radius, w, t the width and thickness and N the number of windings of the coil. Estimating the parameters as $r = 5\,\text{cm}$, $w = t = 1\,\text{cm}$ and $N = 22$, yields $L = 56\,\mu\text{H}$. A more accurate COMSOL simulation of the coil (performed by Giacomo Bisson) yields a value of $L = 15.6\,\mu\text{H}$. Because of different cables used for the different current sources the resistances of the circuit vary. This in turn results in different expected cut-off frequencies. For both the Delta and EA power supplies a direct measurement of the resistance is possible by reading of the voltage and current. In the case of the HF only a current reading is provided. Knowing the cable resistance of the cables $r = 0.7\,\text{m}\Omega/\text{m}$ and a provided cable length of about $l = 4\,\text{m}$ we can estimate the resistance. The resistances and associated cut-off frequencies are summarized in Table 1

Table 1: Summary of primary RL circuit parameters.

Current Source	R[mΩ]	L[µH]	ω_c[Hz]
High-Finesse	≈9	15.6	580
Delta	7	15.6	450
EA	11.1	15.6	700

We will find that the low-pass behaviour is present in the noise measurement in the Delta power supply, but doesn't appear in the case of the EA and HF power supplies. In the linear spectral

noise densities presented later a low-pass noise profile is indicated. Note, the low-pass filter would act as a multiplication of the transfer function (Eq. 5) with the actual noise spectrum. The absolute value of the indicated low-pass filter does not carry any meaning. However, a matching slope in the log-log plot indicates the low-pass filter affecting the measured noise spectrum.

2.3.2 Measurement Noise

Besides the current noise in the primary current the measurement set-up contains some further sources of noise. These include Johnson noise of the shunt resistor, amplifier noise, digitization noise of the oscilloscope and transducer noise. We will now discuss their relative contributions. Note, that if noise is provided in terms of voltage the equivalent current noise can be obtained by means of the proportionality factor in Equation (1). This factor differs due to applied gain factor A and number of primary windings N_p between measurements

Johnson Noise characterizes the thermal noise of a resistor. The resistance in the primary circuit is negligible ($7\,\mathrm{m\Omega}$) compared to the shunt resistor ($25\,\Omega$). The voltage noise added is described by the white-noise power spectral density

$$S_{UU}^{R}(f) = 4k_B T R \tag{7}$$

During the preamplifier stage there is some **amplification noise** added which is provided as white noise linear spectral density for different amplifier settings (e.g. low-noise, $A = 10$, $\sqrt{S_{UU}^{\mathrm{amp}}} = 13\,\mathrm{nV}/\sqrt{\mathrm{Hz}}$).

The **digitization noise** is due to the finite length of the output of the analog to digital conversion (ADC) and governed by the least significant bit U_{LSB} of the ADC. The spectral noise density can be approximated as white noise in the frequency interval $[0, f_S/2]$, with a power spectral density of

$$S_{UU}^{\mathrm{dig}} = U_{\mathrm{LSB}}^2 \cdot \frac{\mathrm{NENBW}}{6 f_S} \tag{8}$$

where NENBW (normalized equivalent noise band-width) is another normalization constant related to the chosen window function (Hanning: NENBW = 1.5). As oversampling increases the sampling frequency this effectively reduces the digitization noise. For the PicoScope oversampling is implemented as the "Resolution Enhancement" feature[2]. In the case of 12+2 bit resolution the additional 2 bits are obtained by a 16-fold oversampling.

By far the largest source of noise is noise added by the **transducer**. The noise of the transducer is given in the manual as "RMS noise current 0 ... 10kHz referred to primary" as 1.5ppm (typical) and 4ppm (maximal). The 1.5ppm refer to the noise at full-scale secondary output current. This corresponds to a nominal primary current of 500 A. Assuming the noise power is independent (or at least lower) of the input current and the noise to be described as white noise we can attribute a spectral noise density as

$$S_{II}^{\mathrm{TD}} = \frac{(1.5\,\mathrm{ppm} \cdot 500\,\mathrm{A})^2}{10\,\mathrm{kHz} \cdot N_p^2} = \frac{1}{N_p^2} 5.625 \times 10^{-11}\,\mathrm{I^2/Hz} \tag{9}$$

where again N_p is the number of primary windings. In Figure 4 the theoretical noise is compared to the measured noise at 0 A primary current, for a winding number of $N_p = 6$, $A = 10$ with

[2] https://www.picoauto.com/library/picoscope/resolution-enhance

the sampling settings as described above. From the figure it can be seen that most of the noise can be explained by the transducer. Comparing the integrated noise power of the measured data $P_{\text{measured}} = 1.3 \times 10^{-9}\,\text{A}^2$ and integrated noise of the transducer $P_{\text{transducer}} = 1.6 \times 10^{-12}\,\text{A}^2$ the measured noise power is far lower than the expected noise power. This suggests that the transducer noise is not independent of the primary current. Hence, in the further discussions we will depict both the measured noise floor and theoretical noise floor given by the transducer.

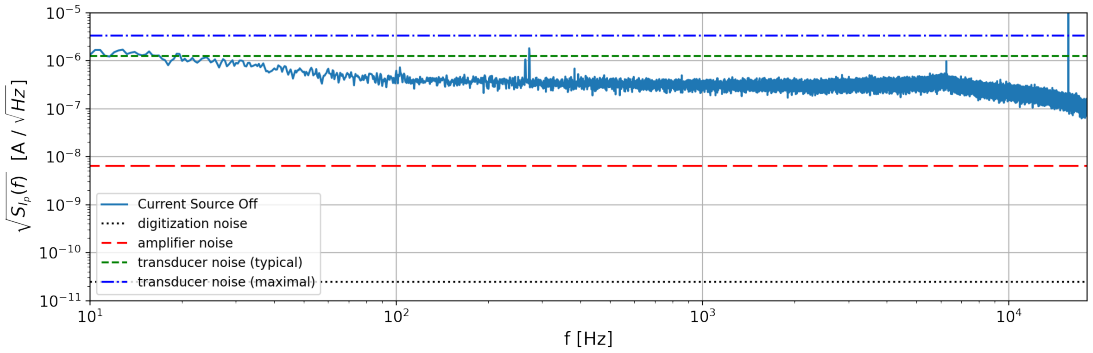

Figure 4: Linear Spectral Density: Measurement Noise at $I_0 = 0\,\text{A}$. Measured noise (blue solid) and theoretical noise (dashed) discussed in text. $A = 10$, $N_p = 6$.

While the noise spectrum is flat in the region 50 Hz to 9000 Hz above 9000 Hz there appears to be another first order low-pass filter. Considering further RL circuits, there are two more candidates. First, the primary current windings around the transducer and second the inductance of the overall circuit loop. The first appears unlikely, as even in the case of the Delta with only a single windings (no loop) through the transducer the behaviour occurs. The second option also appears unlikely, as the HF measurement compared with the Delta measurement had very different areas enclosed by the circuit cables, but display the low-pass behaviour around the same frequency (cf. later sections). The exact reason for this behaviour therefore remains unclear.

2.3.3 Current Source: High-Finesse UCS70

In Figure 6 the linear spectral densities and relative noise distribution for 0 A to 70 A in the frequency range 10 Hz to 18 kHz are shown. The noise profile can be seen to be very flat with only a very weak dependence of the current noise on the set current I_0. All measured values lie about an oder of magnitude above the dark measurement. Interestingly, if the current source is turned on with the current set to 0 A compared to the current at 30 A and 70 A there appears to be a drop in the noise spectrum. This could be explained, as discussed earlier, by a current dependent transducer noise level. The indicated transducer noise level is given at a primary current of i.e. 500 A. The 70 A measurement was performed with 4 primary windings, i.e. an effective 280 A current measured by the transducer. If the current source noise and transducer noise are on the same order of magnitude the low-pass behaviour will not be visible as the transducer noise is added on top the current source noise.

Furthermore, the noise spectrum contains multiple resonances. The resonance at 50 Hz can be identified as the mains frequency. Notably, no second and third harmonics of the mains frequency are visible. There are numerous resonance above 200 Hz, which we did not identify. As can be seen from the cumulative noise power, however, none of the resonances carry much power and can therefore be ignored. Around 12 kHz a broad peak is visible, which most likely is an internal

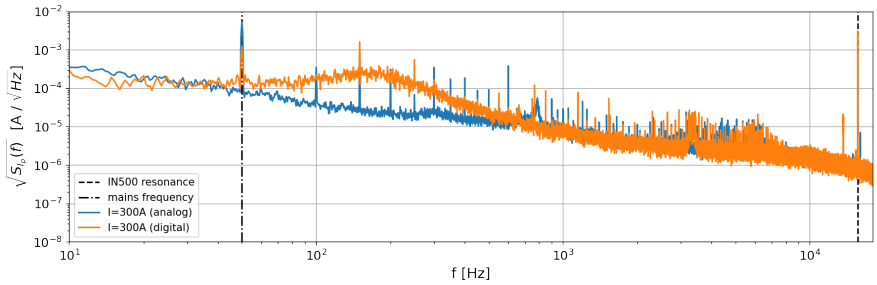

Figure 5: Delta SM-6000: Linear Spectral Density at $I_0 = 300\,\mathrm{A}$ for digital and analog current setting.

resonance of the current source, which also employs a transducer to stabilize the current. Again, as discussed in the measurement noise section there appears a sharp resonance at 15.625 kHz, which is the fluxgate excitation frequency and which will be visible in all further spectral densities as well. Considering, again the cumulative noise power in the case of the HF it turns out that most of the noise can be attributed to the internal resonance of the current source. Here, an additional low-pass filter might be a viable option to significantly reduce the noise. For the 10 Hz - 10 kHz range the integrated current noise at $I_0 = 70\,\mathrm{A}$ is 7.9ppm. This value is still an order of magnitude higher than the noise figure quoted in [3] at 0.67 ppm, even though the above noise figure might be limited by the transducer noise.

2.3.4 Current Source: Delta SM-6000

The linear spectral densities and cumulative noise can for the Delta SM-6000 current source can be found in Figure 7. Comparing the 50 A and 300 A spectrum the noise level appears to be approximately independent of the set current. Different to the HF current source the low-pass filter of the RF circuit is clearly visible. For the resonance the first and higher order harmonics of the mains frequency are visible. Interestingly, considering the cumulative noise, most of the noise in the spectrum can be attributed to the mains frequency. The noise figure at a maximal current of $I_0 = 300\,\mathrm{A}$ in the frequency range 10 Hz - 10 kHz is 14.6ppm. When removing the mains frequency the integrated noise is significantly less at 5.2ppm.

In case of the Delta current source it was possible to either set the current by an analogue control on the front panel of the device or digitally by connecting to the device via an ETH interface. In Figure 5 the noise spectra in the case of the analogue and digital setting at a current of $I_0 = 300\,\mathrm{A}$ are shown. The noise spectra differ with more noise present in the 50 Hz-600 Hz range if the current is set digitally. For the digital setting the mains frequency peak is, however, attenuated. The integrated noise for the analog and digital setting 10 Hz - 10 kHz is 14.6ppm and 11.9ppm respectively. If the mains frequency peak is excluded the noise reduced to 5.2ppm and 11.5ppm respectively.

2.3.5 Current Source: EA 9080-100

For the EA 9080-100 current source the linear spectral density and cumulative noise can be found in Figure 8. For frequencies above 700 Hz we again find the low-pass filter behaviour. The broad resonance at 400 Hz is most likely a resonance within the power-supply, as no such resonant behaviour is visible for the two other power-supplies.

The noise power in the case of the EA appears to be mainly due to higher harmonics of the mains frequency. Integrated the noise of the EA at maximum current $I_0 = 100\,\mathrm{A}$ over the same frequency interval as for the other current sources is 82ppm. We will now compare some of the features of the three power supplies.

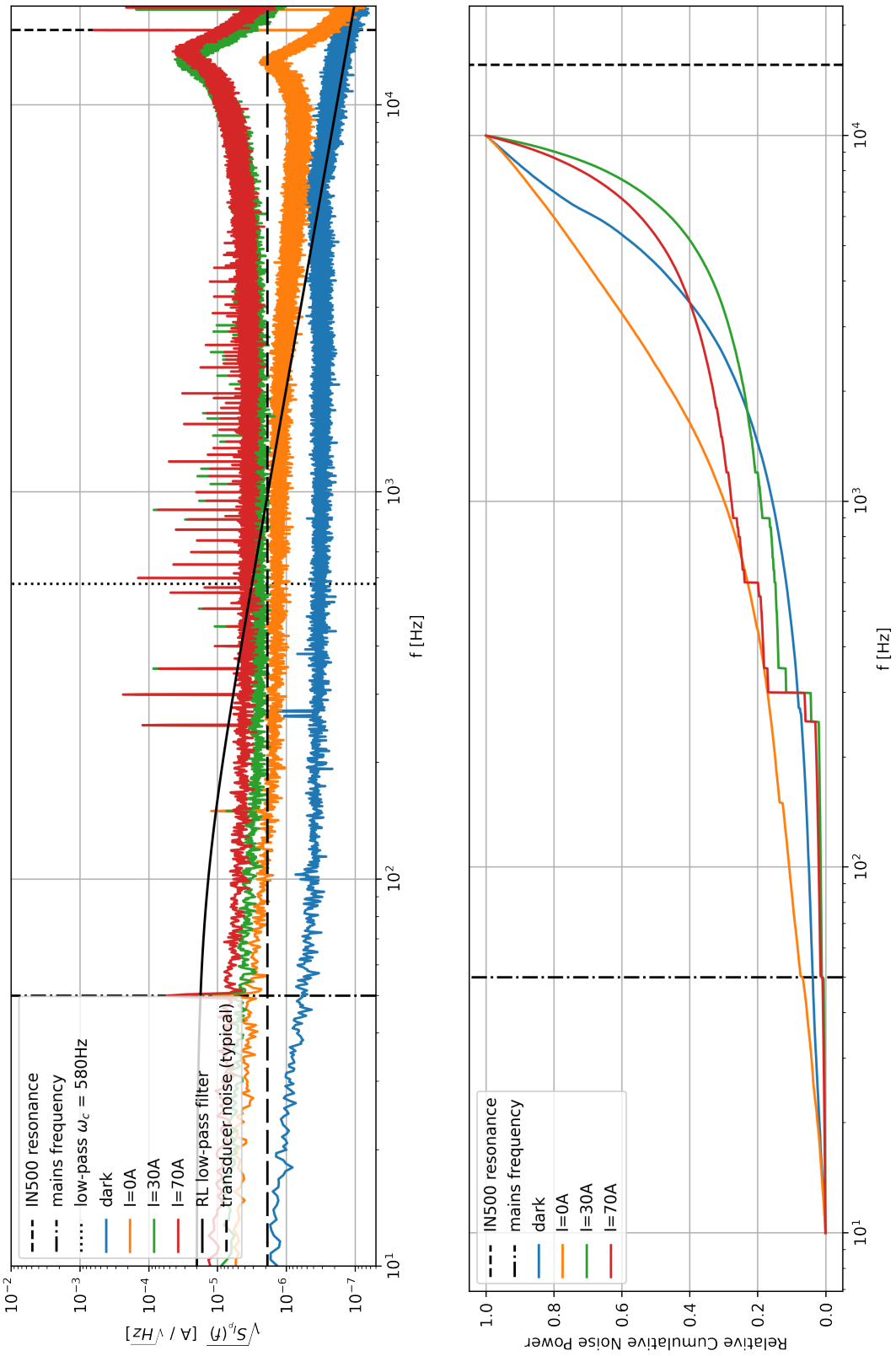

(a) Linear Spectral Density (b) Relative Cumulative Noise Power

Figure 6: High-Finesse UCS70. Measurement Settings: $A = 10$, $N_p = 6$

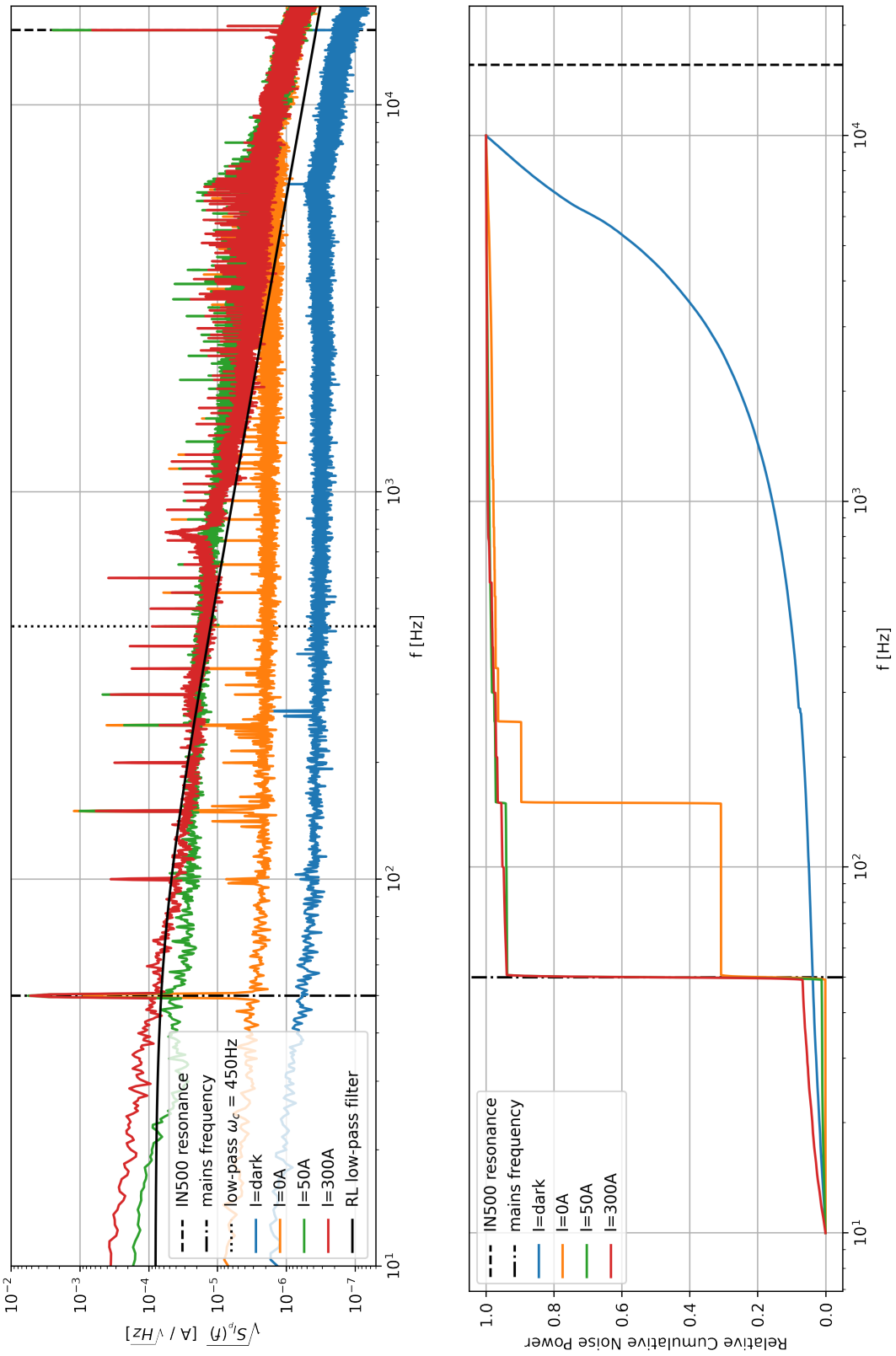

(a) Linear Spectral Density (b) Relative Cumulative Noise Power

Figure 7: Delta SM-6000. Measurement Settings: $A = 10$, $N_p = 1$

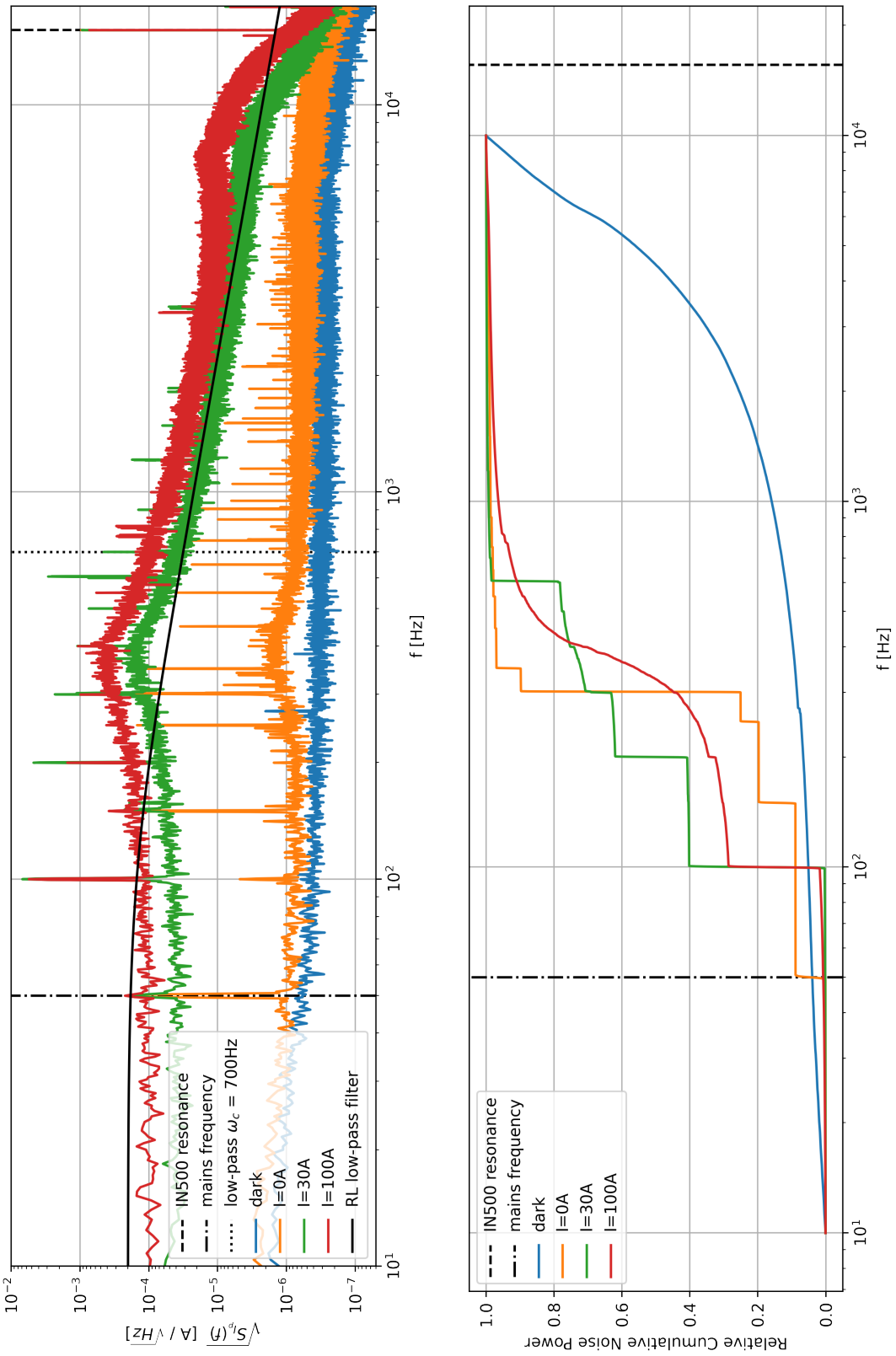

(a) Linear Spectral Density (b) Relative Cumulative Noise Power

Figure 8: EA 9080-100. Measurement Settings: $A = 10$, $N_p = 3$

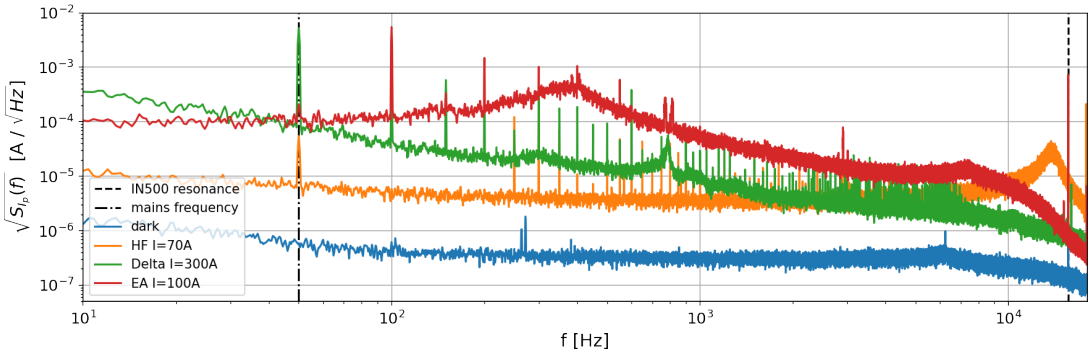

Figure 9: Linear Spectral Density of three different current sources at maximum current.

2.3.6 Current Sources: Comparison

Last we want to compare the different current sources. The linear spectral densities of the three current sources are shown in Figure 9. The current source with the lowest overall noise is the High-Finesse current source, with an integrated noise of 7.9ppm. However, due to the broad resonance at higher frequencies in the High Finesse the Delta current source has a comparable noise level above 2 kHz. The EA has an overall larger noise compared to the other two current sources with an integrated noise of about 82ppm, even though at low frequency it appears to be slightly more stable than the Delta current source. Given the noise level of the current sources and depending on the application of the current source it might be necessary to reduce the noise further by high-pass filtering if possible or implement feedback and feedforward mechanisms. A limiting factor for the later might be the noise level of the transducer.

For the both the High-Finesse and Delta current noise figures are provided. In the case of the High-Finesse a current shunt measurement was performed. Here the current noise for the bandwidth 10 kHz at 60 A was given as 7 mA and 5 mA for two different shunt resistors. This would correspond to a lower noise figure of 71ppm assuming the integrated noise power is the same at 70 A. This is an order of magnitude above the figure obtained in our measurement.
The noise figure provided for the Delta power supply at a bandwidth of 300 kHz at full output in current control is $I_{\text{noise}} = 100mA$. To compare this figure with our measurement we assume the noise density to decrease for higher frequency. We can then give an upper limit on the noise in the 10 kHz bandwidth. This yields a noise current of 18 mA corresponding to about 60ppm at 300 A. This figure is again about an order of magnitude above our obtained value. This leads us to conclude that the influence of the RL low-pass behaviour suppresses significant amount of noise. Because the Delta power supply will be used to power the coil installed in the primary circuit the measured spectrum hence represents the noise spectrum of the coil. In the case of the other power supplies the spectrum will look different if another instrument is connected instead. To improve on the above results it would be enough to replace the coil by a resistor in the measurement set-up.

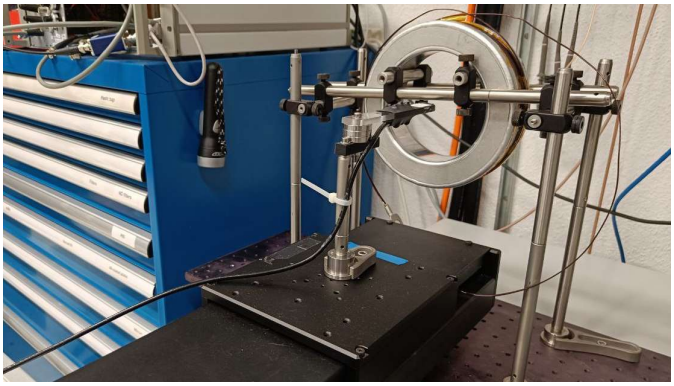

Figure 10: Magnetic field measurement set-up. The magnetic field is measured along the direction of the Hall probe.

3 Magnetic Field Measurement

In this section we describe the magnetic field measurements for the four MOT coils. We show that the z-axis magnetic field is well described by a simple current loop model. We also show measurements of the stray-fields.

3.1 Measurement Set-up

To measure the magnetic field coils we used a DTM 151 digital Teslameter, which provided a Hall sensor to measure the magnetic field perpendicular to the sensor surface. The sensor was mounted on top of a rail which could be moved by an ODrive motor. The sensors outputs could be read out via an GPIB interface. With this set-up it was possible to take magnetic field measurements along single linear directions.

For each position the magnetic field was determined as the mean of three measurements taken in the span of < 1s. Before each measurement a dark reading was taken with the coil current switched off, which was deducted from the coil magnetic field readings.

3.2 Results

In Figure 11 the B_z is shown for the four coils along the z-direction which was taken to be the center axis of symmetry of the MOT coils. The theory provides a prediction with only one free parameter for the center of the coil z_0 along the z-axis, given by [4]:

$$B_z = \frac{\mu_0 I a^2}{2\left(a^2 + (z - z_0)^2\right)^{3/2}} \tag{10}$$

with current $I = 110 \times 15\,\mathrm{A}$ and $a = 7.4\,\mathrm{cm}$ the average radius of the windings. As can be seen in Figure 11 the theory is in good agreement with the measurement.

To estimate the stray fields of the coils we measured the magnetic field components along the radial direction. The results are shown in Figure 12. As expected the B_z component is largest, while the angular component almost vanishes B_ϕ. The B_r component measurement is far more

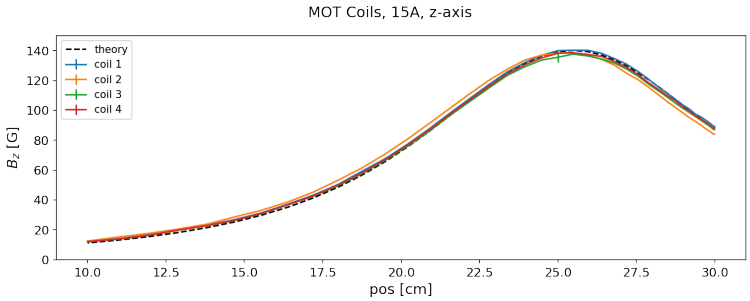

Figure 11: MOT coil magnetic field measurement: B_z component along z direction. Measurements (solid lines), theory (dashed lines).

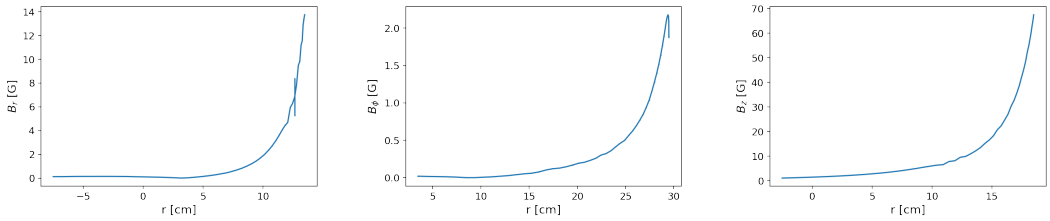

(a) B_r (b) B_ϕ (c) B_z

Figure 12: MOT coil stray magnetic field along radial direction.

susceptible to slight deviations from the radial axis, which explains the large contribution compared to B_z, which would be expected to vanish due to symmetry considerations.

4 Temperature Stability of MOT coils

In this section we want to shortly discuss some observations on the temperature stability of the MOT coils. The temperature was measured by IR camera images and temperature measurements of the cooling water. In Figure 13 both the temperature and flow measurements are shown for a current of 15 A. At 14:35 the current was increased from 10 A and run until 15:15. The water temperature before the coil was run was 17.0 °C. A different temperature measurement of the chiller read 19.2 °C at this time, which suggests an absolute error in the water temperature reading. The steady-state temperature for a flow of $v_w = 1.5\,\mathrm{l/min}$ was 17.8 °C. The power dissipated in the coil ($R = 0.4\,\Omega$) is given by

$$P_{\mathrm{coil}} = I^2 R = 90\,\mathrm{W} \tag{11}$$

The heat transfer to the water was

$$P_{\mathrm{water}} = C_w (T_1 - T_0) v_w = 82\,\mathrm{W} \tag{12}$$

with C_w the volumetric heat capacity. Hence, most of the heat produced by the coil heat dissipated by the water. Furthermore, as shown for example in Figure 14 we could examine the temperature distribution across the coil. As can be seen in the figure no local temperature hot

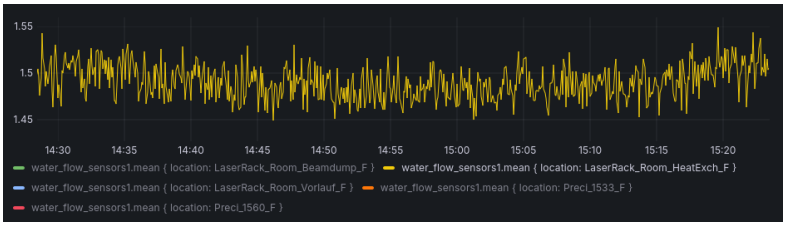

(a) Water flow in l/min.

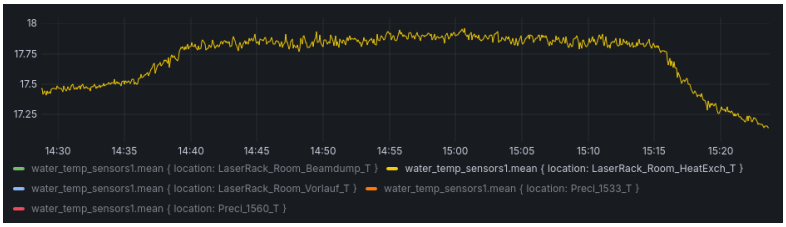

(b) Water temperature in °C.

Figure 13: Water flow and temperature measurement for the MOT coil at $I = 15\,\mathrm{A}$.

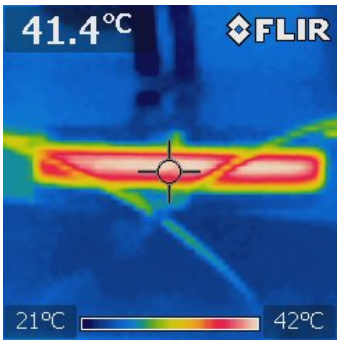

Figure 14: Infrared temperature profile of MOT coil for reflectivity $\epsilon = 0.95$ at $I = 15\,\mathrm{A}$.

spots were detected. This was consistent throughout the whole 45min of operation. The absolute temperature reading in the IR picture is not very reliable as it depends highly on the chosen reflectivity.

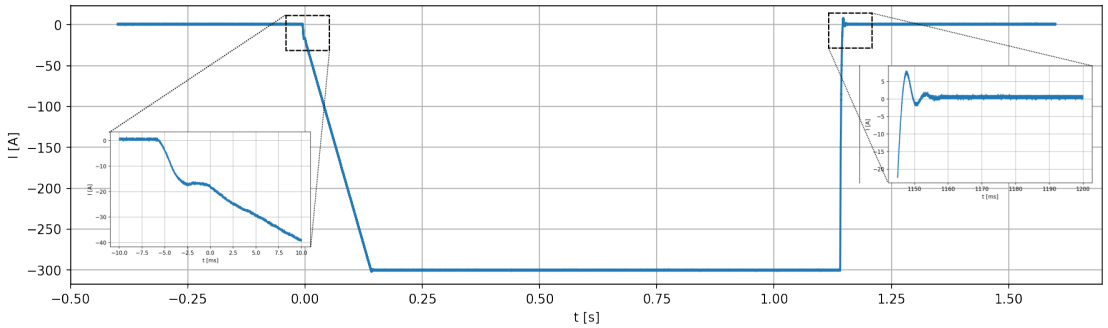

Figure 15: Delta SM-6000 current ramp sequence 300A/100ms. Insets show features at start and end of ramp.

5 Programming Current Ramp Sequences

Last, we implemented and characterized a simple current ramp for the Delta SM-6000 power supply. The ramp was implemented in the power-supply specific SEQUENCER syntax. The code could be loaded and executed from the web-interface via an ETH connection. The code can also be executed by sending a 1 (5V) signal to the CON F user input A. The delay between the input signal and start of sequence was not measured. The code to run a ramp from 0 to 300A in 100ms is

`RAMPCURRENT.seq`

```
1 sv=0 # set voltage to 0V
2 sc=0 # set current to 0A
3 w=1  # wait 1 second
4 sv=1 # set voltage to 1V
5 cjg sc,300,9 # if current is 300 jump to step 9
6 inc sc,3 # increment current by 3A
7 w=0.001 # wait 1ms
8 jp 5 # jump to 5 (i.e. repeat current check and increment)
9 w=1 # wait 1 second
10 sv=0 # set voltage to 0V
11 sc=0 set current to 0A
12 end # end sequence
```

Note, comments are not allowed in the sequences and need to be removed. The minimum wait time is limited to 1ms which sets the minimum increment for this ramp to 3A. The current was measured with the same set-up used for the current noise measurements, but with the amplifier removed. The result is shown in Figure 15. The ramp does indeed ramp linearly from 0A to 300A, with some small ringing at the beginning and end of the ramp. We also determined the ramp velocity by a linear fit between 0.0s and 0.14s. The resultant ramp speed is determined as 200 A/100ms, a third slower than expected. This suggests that the execution of the conditional jump step (5) and increment step (6) do add a significant lag as well. This would need to be taken into consideration in a future implementation.

6 References

[1] Miguel Cerqueira Bastos et al. "High accuracy current measurement in the main power converters of the large hadron collider: tutorial 53". In: *IEEE Instrumentation & Measurement Magazine* 17.1 (Feb. 2014), pp. 66–73. ISSN: 1941-0123. DOI: 10.1109/MIM.2014.6783001. URL: https://ieeexplore.ieee.org/document/6783001 (visited on 07/11/2024).

[2] G. Heinzel, A. Rüdiger, and R. Schilling. *Spectrum and spectral density estimation by the Discrete Fourier transform (DFT),* tech. rep. Max-Planck-Institut für Gravitationsphysik, Feb. 2002. URL: http://holometer.fnal.gov/GH_FFT.pdf.

[3] B. Merkel et al. "Magnetic field stabilization system for atomic physics experiments". In: *Review of Scientific Instruments* 90.4 (Apr. 2019), p. 044702. ISSN: 0034-6748. DOI: 10.1063/1.5080093. URL: https://doi.org/10.1063/1.5080093 (visited on 07/16/2024).

[4] James C. Simpson et al. *Simple Analytic Expressions for the Magnetic Field of a Circular Current Loop.* Tech. rep. NASA/TM-2013-217919. NTRS Author Affiliations: NASA Kennedy Space Center, DYNACS Engineering Co., Inc. NTRS Document ID: 20140002333 NTRS Research Center: Kennedy Space Center (KSC). Feb. 2001. URL: https://ntrs.nasa.gov/citations/20140002333 (visited on 05/13/2024).

[5] H.A. Wheeler. "Simple Inductance Formulas for Radio Coils". In: *Proceedings of the Institute of Radio Engineers* 16.10 (Oct. 1928), pp. 1398–1400. ISSN: 2162-6626. DOI: 10.1109/JRPROC.1928.221309. URL: https://ieeexplore.ieee.org/document/1669896 (visited on 07/13/2024).

Eidgenössische Technische Hochschule Zürich
Swiss Federal Institute of Technology Zurich

Declaration of originality

The signed declaration of originality is a component of every written paper or thesis authored during the course of studies. In consultation with the supervisor, one of the following three options must be selected:

I confirm that I authored the work in question independently and in my own words, i.e. that no one helped me to author it. Suggestions from the supervisor regarding language and content are excepted. I used no generative artificial intelligence technologies[1].

I confirm that I authored the work in question independently and in my own words, i.e. that no one helped me to author it. Suggestions from the supervisor regarding language and content are excepted. I used and cited generative artificial intelligence technologies[2].

I confirm that I authored the work in question independently and in my own words, i.e. that no one helped me to author it. Suggestions from the supervisor regarding language and content are excepted. I used generative artificial intelligence technologies[3]. In consultation with the supervisor, I did not cite them.

Title of paper or thesis:

Authored by:
If the work was compiled in a group, the names of all authors are required.

Last name(s): **First name(s):**

With my signature I confirm the following:
- I have adhered to the rules set out in the Citation Guide.
- I have documented all methods, data and processes truthfully and fully.
- I have mentioned all persons who were significant facilitators of the work.

I am aware that the work may be screened electronically for originality.

Place, date **Signature(s)**

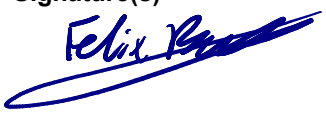

If the work was compiled in a group, the names of all authors are required. Through their signatures they vouch jointly for the entire content of the written work.

[1] E.g. ChatGPT, DALL E 2, Google Bard
[2] E.g. ChatGPT, DALL E 2, Google Bard
[3] E.g. ChatGPT, DALL E 2, Google Bard